



Extrinsic chirality of non-concentric plasmonic nanorings

VLADIMIR E. BOCHENKOV,^{1,3} GUNNAR KLÖS,² AND DUNCAN S. SUTHERLAND^{2,4}

¹*Department of Chemistry, Lomonosov Moscow State University, Moscow, Russia*

²*Interdisciplinary Nanoscience Center (iNANO), Aarhus University, Aarhus, Denmark*

³*boch@kinet.chem.msu.ru*

⁴*duncan@inano.au.dk*

Abstract: We show how extrinsic chirality, i.e. the optical activity of achiral media exhibited at oblique light incidence, can be achieved in plasmonic nanorings by symmetry breaking. We demonstrate that even a small, 5% offset of an inner hole of a 190 nm gold ring results in a measurable circular dichroism signal in the near-infrared region. By using computer simulations, we show that optical activity arises upon excitation of a symmetric dipolar localized surface plasmon resonance mode due to the appearance of co-aligned electric and magnetic dipole moments.

© 2017 Optical Society of America

OCIS codes: (250.5403) Plasmonics; (160.4236) Nanomaterials.

References and links

1. W. Lenz, "Malformations caused by drugs in pregnancy," *Am. J. Dis. Child.* **112**, 99–106 (1966).
2. E. Hendry, T. Carpy, J. Johnston, M. Popland, R. V. Mikhaylovskiy, A. J. Lapthorn, S. M. Kelly, L. D. Barron, N. Gadegaard, and M. Kadodwala, "Ultrasensitive detection and characterization of biomolecules using superchiral fields," *Nature Nanotech.* **5**, 783–787 (2010).
3. A. Ben-Moshe, B. M. Maoz, A. O. Govorov, and G. Markovich, "Chirality and chiroptical effects in inorganic nanocrystal systems with plasmon and exciton resonances," *Chem. Soc. Rev.* **42**, 7028–7041 (2013).
4. H. Zhang and A. O. Govorov, "Giant circular dichroism of a molecule in a region of strong plasmon resonances between two neighboring gold nanocrystals," *Phys. Rev. B* **87**, 075410 (2013).
5. W. Ma, H. Kuang, L. Wang, L. Xu, W. S. Chang, H. Zhang, M. Sun, Y. Zhu, Y. Zhao, L. Liu, C. Xu, S. Link, and N. A. Kotov, "Chiral plasmonics of self-assembled nanorod dimers," *Sci. Rep.* **3**, 1934 (2013).
6. Z. Wang, F. Cheng, T. Winsor, and Y. Liu, "Optical chiral metamaterials: a review of the fundamentals, fabrication methods and applications," *Nanotechnology* **27**, 412001 (2016).
7. M. Hentschel, M. Schäferling, X. Duan, H. Giessen, and N. Liu, "Chiral plasmonics," *Science Advances* **3**, e1602735 (2017).
8. A. Kuzyk, R. Schreiber, Z. Y. Fan, G. Pardatscher, E. M. Roller, A. Hoge, F. C. Simmel, A. O. Govorov, and T. Liedl, "Dna-based self-assembly of chiral plasmonic nanostructures with tailored optical response," *Nature* **483**, 311–314 (2012).
9. W. Ma, H. Kuang, L. Xu, L. Ding, C. Xu, L. Wang, and N. A. Kotov, "Attomolar dna detection with chiral nanorod assemblies," *Nat. Commun.* **4**, 2689 (2013).
10. M. Hentschel, L. Wu, M. Schäferling, P. Bai, E. P. Li, and H. Giessen, "Optical properties of chiral three-dimensional plasmonic oligomers at the onset of charge-transfer plasmons," *ACS Nano* **6**, 10355–10365 (2012).
11. M. Hentschel, M. Schäferling, T. Weiss, N. Liu, and H. Giessen, "Three-dimensional chiral plasmonic oligomers," *Nano Lett.* **12**, 2542–2547 (2012).
12. E. Plum, "Extrinsic chirality: Tunable optically active reflectors and perfect absorbers," *App. Phys. Lett.* **108**, 241905 (2016).
13. I. Sersic, M. A. van de Haar, F. B. Arango, and A. F. Koenderink, "Ubiquity of optical activity in planar metamaterial scatterers," *Phys. Rev. Lett.* **108**, 223903 (2012).
14. L. Hu, X. Tian, Y. Huang, L. Fang, and Y. Fang, "Quantitatively analyzing the mechanism of giant circular dichroism in extrinsic plasmonic chiral nanostructures by tracking the interplay of electric and magnetic dipoles," *Nanoscale* **8**, 3720–3728 (2016).
15. X. Ma, M. Pu, X. Li, Y. Guo, P. Gao, and X. Luo, "Meta-chirality: Fundamentals, construction and applications," *Nanomaterials* **7**, 116 (2017).
16. E. Plum, X. X. Liu, V. A. Fedotov, Y. Chen, D. P. Tsai, and N. I. Zheludev, "Metamaterials: Optical activity without chirality," *Phys. Rev. Lett.* **102**, 113902 (2009).
17. J. H. Shi, Z. Zhu, H. F. Ma, W. X. Jiang, and T. J. Cui, "Tunable symmetric and asymmetric resonances in an asymmetrical split-ring metamaterial," *J. Appl. Phys.* **112**, 073522 (2012).

18. C. Feng, Z. B. Wang, S. Lee, J. Jiao, and L. Li, "Giant circular dichroism in extrinsic chiral metamaterials excited by off-normal incident laser beams," *Opt. Commun.* **285**, 2750–2754 (2012).
19. X. Lu, J. Wu, Q. Zhu, J. Zhao, Q. Wang, L. Zhan, and W. Ni, "Circular dichroism from single plasmonic nanostructures with extrinsic chirality," *Nanoscale* **6**, 14244–14253 (2014).
20. L. Hu, Y. Huang, L. Fang, G. Chen, H. Wei, and Y. Fang, "Fano resonance assisting plasmonic circular dichroism from nanorice heterodimers for extrinsic chirality," *Sci. Rep.* **5**, 16069 (2015).
21. V. E. Bochenkov and D. S. Sutherland, "From rings to crescents: a novel fabrication technique uncovers the transition details," *Nano Lett.* **13**, 1216–1220 (2013).
22. P. Hanarp, D. S. Sutherland, J. Gold, and B. Kasemo, "Control of nanoparticle film structure for colloidal lithography," *Coll. Surf. A* **214**, 23 – 36 (2003).
23. P. B. Johnson and R. W. Christy, "Optical constants of noble metals," *Phys. Rev. B* **6**, 4370–4379 (1972).
24. V. A. Fedotov, P. L. Mladyonov, S. L. Prosvirnin, A. V. Rogacheva, Y. Chen, and N. I. Zheludev, "Asymmetric propagation of electromagnetic waves through a planar chiral structure," *Phys. Rev. Lett.* **97**, 167401 (2006).

1. Introduction

Chirality is one of the fundamental characteristics of symmetry: chiral shape cannot be superimposed onto its own mirror image. Most biologically relevant molecules are chiral, including the primary biological building blocks — sugars and aminoacids. Chirality can be crucially important, especially in pharmaceuticals, where an enantiomer of a drug molecule, i.e. one having the same composition but the opposite handedness, can have no therapeutic effect or can even be toxic [1]. Thus, correct determination of molecular chirality is vital in biomedical diagnostics and for pathogen detection [2]. One of the commonly used methods for studying molecular chirality is the circular dichroism (CD) spectroscopy, which is based on different absorption of right- and left- circularly polarized light by chiral media. Unfortunately, the typical CD signals are very weak and become detectable only when a large number of optically active molecules interact with light upon its propagation. A potential advancement in this field is associated with the use of chiral plasmonic structures, which due to strong interaction with light are capable of generating superchiral local fields and hence lowering detection limits of chiral sensors [2–6].

A number of chiral plasmonic systems has been studied so far [7]. In addition to *intrinsically* chiral 3D structures [2, 8] and oligomers [5, 9–11], a new class of *extrinsically* chiral planar plasmonic systems has recently been discovered. Extrinsic chirality is found in achiral plasmonic structures under oblique illumination conditions, when the light propagation vector and the structure make an arrangement that is 3D chiral [12]. It results from a strong interplay between electric and magnetic dipoles, leading to mixed electric and magnetic polarizability [13, 14]. Strong optical activity and high tunability make such structures favorable candidates for a number of applications, including polarization detection and imaging [15]. So far, extrinsic chirality has been demonstrated for a number of plasmonic structures, including split-rings [16–18], nanorod dimers [19], nanorice heterodimers [20], *etc.*

Most of these systems rely upon the precision of the 'top-down' approaches, such as Electron Beam Lithography or Focused Ion Beam lithography. Here, we present a new extrinsically chiral metamaterial fabricated by self-assembly-based colloidal lithography approach. We show both experimentally and by using a computer simulation that extrinsic chirality can be successfully achieved in plasmonic nanorings by symmetry breaking. The optical activity in non-concentric rings (NCRs) under oblique light illumination results from the non-zero projection of magnetic and electric moments on the plane normal to wave propagation.

2. Results and discussion

2.1. Fabrication of non-concentric rings

Irregular arrays of gold NCRs have been fabricated on glass and silicon substrates using our recently developed In-situ Resist Colloidal Lithography technique [21], as depicted in Fig. 1(a). In this approach, both the adsorbed colloidal particles and the silica resist layer are used as a

mask for patterning the ring structures. The procedure involved the following steps. First, Si or glass substrates have been cleaned by ultrasonication in acetone, ethanol and Milli-Q water (10 min each) followed by 30-minute UV/ozone oxidation. Next, polyelectrolyte triple layer has been formed using the solutions of PDDA (Poly(diallyldimethylammonium chloride), 2% wt, 30 sec), PSS (Poly(sodium 4-styrenesulfonate), 2% wt, 30 sec) and PAX (Polyaluminium chloride, 5 % wt, 30 sec). Then, 200 nm sulfate latex microspheres (Invitrogen, USA) have been deposited from 0.2% wt solution in Milli-Q water to create a characteristic pattern used in sparse colloidal lithography methods [22]. After rinsing with Milli-Q water and drying in nitrogen flow, the samples have been stored at ambient conditions. Right before vacuum deposition, the samples were treated for 3 min by UV/ozone to remove polyelectrolyte layers and improve adhesion.

Vacuum deposition has been carried out in the following order: (I) Ti (2 nm, at 45° with 5 rpm), (II) silica (25 nm, at 5° with no rotation) and (III) Au (20 nm, at 40° with 1 rpm) using e-beam evaporation in a PVD system Cryofox Explorer 500 GLAD (Polyteknik, Denmark). After the deposition, samples have been taken out to air, and both the microspheres and the top layer of gold have been removed by repeated tape stripping using a cleanroom adhesive tape. Since NCRs height is less than the thickness of the silica film, and due to the Ti adhesion layer, the structures remain intact at the bottom of the holes in SiO_2 after this procedure. For comparison, concentric rings have been fabricated using the same procedure, but with normal (0°) deposition of silica resist layer in the step II (data not shown).

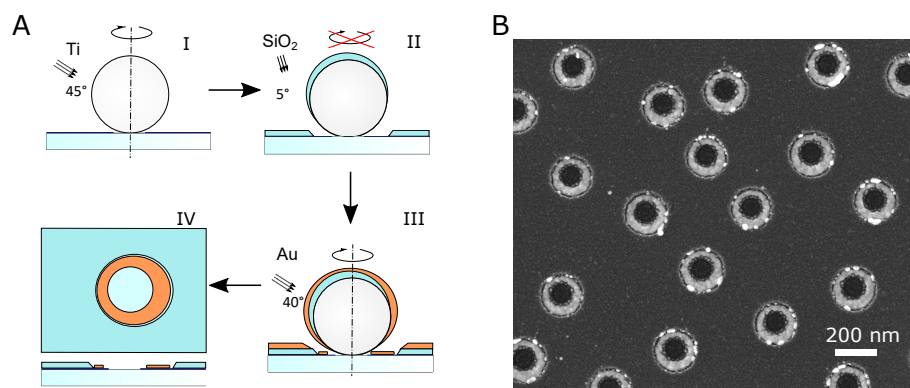


Fig. 1. Non-concentric nanorings: A) fabrication using In-Situ Resist Colloidal Lithography: I) deposition of Ti adhesion layer, II) deposition of silica resist layer, III) deposition of gold, IV) asymmetric ring structure after removal of particles and top gold layer (top view and cross-section); B) scanning electron microscopy image of NCRs on Si substrate.

According to SEM data (see Fig. 1(b)), the particles are uniformly distributed across the surface with short-range (but no long-range) order. The NCRs have outer diameter of about 190 nm, inner diameter of about 120 nm, and a hole offset of 10 nm, which is about 5% of the ring size. The particles are all oriented in the same way, i.e. have symmetry axis parallel to each other. It should be noted that with higher deposition angles of silica resist layer the larger offset is potentially possible; however, for the 190 nm diameter NCRs offsets larger than 10 nm lead to cracking in the thin part of the rings.

2.2. Optical properties of non-concentric rings

Optical properties of plasmonic nanoring arrays have been experimentally studied using UV-vis/NIR spectrometer (Shimadzu 3600, Japan). CD measurements have been carried out using a custom-built optical system involving a linear polarizer and a quarter-wave plate (Thorlabs, USA), installed in front of a sample in the sample chamber of the spectrometer. The extinction (1-T)

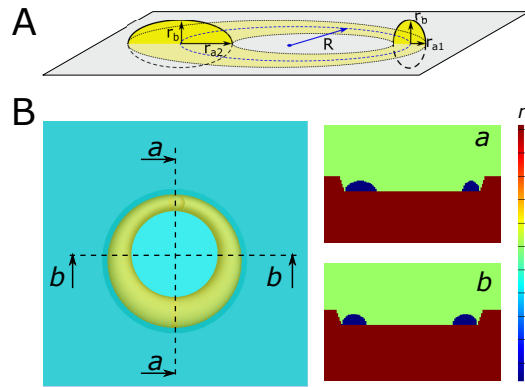


Fig. 2. Non-concentric ring model: A) construction schematics; B) top view and cross-sections of the geometry used in FDTD simulations

spectra at different tilt angle in right- or left- circularly polarized light (A_R and A_L , respectively) have been registered using a single beam mode with a clean glass slide as a reference.

To support the experiment, the finite-difference time-domain (FDTD) simulations of optical response of a single NCR structure on a glass substrate have been carried out using the full 3D Maxwell solver FDTD Solutions (Lumerical, Canada) with perfectly matched layers as boundary conditions. NCR model shape was constructed by sweeping an ellipsis with radius r_a that is parallel to the NCR plane and radius r_b perpendicular to it around a circular contour with radius $R = 78$ nm. Radius $r_b = 14$ nm defines the ring's height and is constant, while r_a is gradually changed from $r_{a1} = 12$ nm at the top to $r_{a2} = 22$ nm at the bottom side of the NCR. The offset between the hole and the outer edge of the ring equals to $r_{a2} - r_{a1} = 10$ nm. The bottom part of the NCR is cut to the center of an ellipsis. The ring is placed on a substrate inside a truncated conical well, representing experimental conditions. The resulting NCR dimensions matched those determined from the SEM images. The dielectric function of gold used in these simulations was obtained by fitting the experimental data from Johnson and Christy [23]. Constant refractive index $n=1.52$ was used for glass. The mesh size in the region containing the NCR was 1 nm. The model is depicted in Fig. 2.

As depicted in Fig.3, the extinction (1-T) spectrum of NCRs in non-polarized light contains three peaks, corresponding to the low-energy symmetric dipole LSPR mode at 1550 nm, high-energy anti-symmetric mode at 600 nm and the quadrupole mode at 1000 nm, which is known to become visible due to symmetry breaking [21]. The peak positions in the simulated extinction spectrum are in a good agreement with the experimental results. The larger width of the peaks in the experimental spectra can be explained by inhomogeneous broadening due to polydispersity of particle size and shape.

CD spectra have been obtained as an extinction difference: $\Delta = (A_R - A_L)$. Due to the limited spectral working range of the used quarter-wave plate, the CD spectra were obtained for the range 1100–1630 nm, which covered the most intensive low-energy peak. The experimental extinction and CD spectra of NCRs registered at $+30^\circ$, 0° and -30° tilt across the symmetry axis are presented in Fig. 3(b) (left column) accompanied by the corresponding simulated spectra (right column). We found that NCRs demonstrate significant circular dichroism at the frequency corresponding to the dipolar LSPR mode when illuminated at oblique angle. The absolute value of CD reached a maximum when sample was tilted across the axis parallel to the symmetry axis of the NCRs while it vanished at normal illumination, or when the sample was tilted across the perpendicular axis. The CD spectrum changed its sign when the tilting angle was changed to the opposite. The optical properties were identical for the illumination from the substrate and from

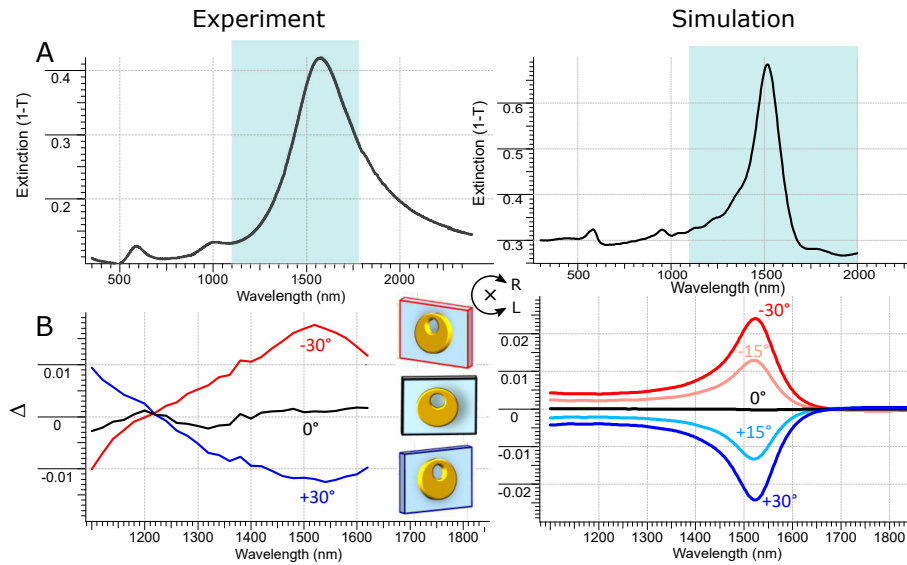


Fig. 3. Spectral properties of plasmonic NCRs: experiment (left column) and simulation (right column). (A) Extinction (1-T) spectra obtained in non-polarized light. The region used to analyze the circular dichroism is marked with light-blue color. (B) Extinction difference between right- and left-handed circularly polarized light ($\Delta = A_R - A_L$) obtained with the sample tilted across the axis parallel to the symmetry axis. The orientations for positive, negative and no tilt angle are shown.

the air, showing no asymmetric transmission effect characteristic for chiral 2D structures [24]. Registered at the same conditions, extinction spectra of concentric rings demonstrate no difference for left- and right circular polarization of incident light, thus giving no CD signal, independently of sample tilt (not shown).

Simulated CD response generally matched the experimental results, showing the same behavior near the resonance wavelength with respect to tilt. The observed discrepancy in the region below 1200 nm is not completely understood and can be attributed either to the imperfections of the FDTD model not reproducing the peculiarities of the NCR's shape, or to the poor performance of the used optical parts near the edge of their working region.

2.3. Mechanism of the optical activity

To understand the optical activity of tilted NCRs, we first take a closer look at the lowest-energy plasmon mode of a nanoring, see Fig. 4. Since circularly polarized light can be represented by two light waves with orthogonal polarization and 90° phase shift, it is convenient to consider plasmon excitation by two linearly polarized light waves independently. Upon excitation of the symmetric LSPR dipole mode, electrons oscillate across the metallic structure in the direction of light polarization, traveling by trajectories with curvature radius defined by the diameter of the ring.

In case of a concentric ring or a non-concentric ring with its offset axis oriented parallel to the light polarization vector the oscillating electric current created by the charges moving clockwise has the equivalent flow of counter-clockwise moving charges. The induced magnetic moments cancel out and no net magnetic moment appears.

In case of NCR, the two channels become inequivalent and more charges move in one arch of the ring than in the other, as illustrated by Fig 4(b). The uncompensated oscillating current induces net magnetic moment \mathbf{M} normal to the plane of the ring. The dynamics of the calculated

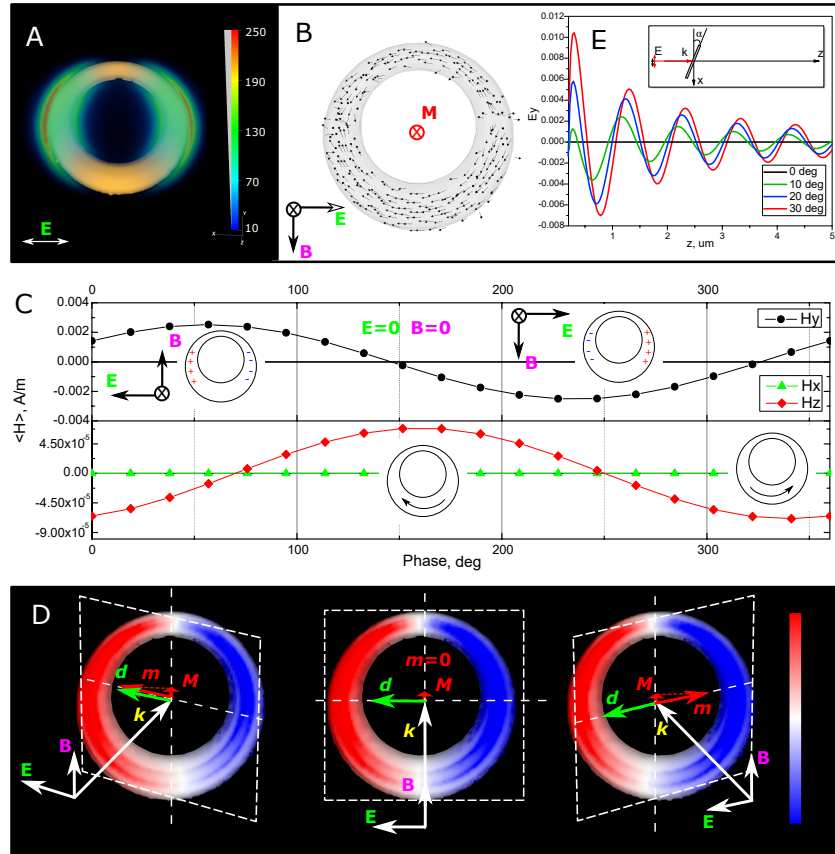


Fig. 4. Low-energy symmetric dipole LSPR mode of gold NCR: A) enhanced local electric field ($|E^2|/|E_0^2|$), B) snapshot of electric currents leading to the net magnetic moment M , C) calculated average magnetic field vector components vs phase (with corresponding instant charge distributions); D) simulated charge plots and schematics of the system upon positive (left), zero (center), and negative (right) angle of incidence, showing the appearance of the non-zero projections of magnetic (m , red arrow) and electric (d , green arrow) moments on the plane normal to propagation vector k ; E) Appearance of the orthogonal component of electric field in transmitted light due to sample tilt. The inset shows the schematics of the model.

average magnetic field vector components is presented in Fig 4(c). H_y component demonstrates the magnetic field caused by the incident electromagnetic wave, also defining the phase of the electric field vector. The H_x component of the field is zero, whereas H_z reaches considerably large values. Importantly, there is a phase lag between the incident wave and the magnetic response, with maximum values of $|H_z|$ corresponding to the highest current flow and near-zero values of H_y , which supports the proposed mechanism.

At oblique light illumination with tilting around Y axis, the projection \mathbf{m} of this magnetic moment on the plane normal to the wave propagation vector \mathbf{k} is non-zero, and is directed either parallel or anti-parallel to the projection of electric dipole \mathbf{d} , depending on the sign of the tilt (see Fig 4(d)). The oscillating dipole moments create a component of a retarded wave with orthogonal polarization. This wave is scattered in the direction of incident light and adds up to the transmitted wave, effectively rotating its polarization plane.

The appearance of the electromagnetic wave component with the orthogonal polarization plane in transmitted light is demonstrated in Fig 4(e). When NCR structure is illuminated with X-polarized light at normal incidence (along Z axis), no orthogonally polarized waves E_y is detected in the transmitted light (black line). Once the structure is tilted, the E_y component appears, with its contribution and phase lag increasing with the tilt angle.

The second component of the circularly-polarized light, i.e. the wave with the polarization along the symmetry axis of the NCR induces only symmetric charge flows, thus it does not lead to an additional magnetic response and does not affect the polarization of transmitted light.

Thus, the CD response of short-range ordered arrays of NCRs observed at oblique illumination is a result of their optical activity that appears because of 1) the formation of the magnetic moment \mathbf{M} by the uncompensated current and 2) the non-zero projection of this moment onto a plane, normal to wave propagation. The interaction between plasmon modes of individual particles is weak, and the optical response of this amorphous 2D metamaterial is well reproduced by simulation of a single NCR structure.

3. Conclusion

We have demonstrated how symmetry breaking in plasmonic nanorings induces extrinsic chirality. Even a small, 5% offset of the ring's hole leads to a pronounced CD signal for 190 nm gold rings. The optical activity arises because the light-driven motion of charges in asymmetric non-concentric nanorings under illumination with circularly polarized light induces an oscillating magnetic moment, oriented perpendicularly to the plane of the ring. Under oblique incidence, the projection of this magnetic moment on the plane normal to the wave propagation is non-zero, with its sign depending on the handedness of the light. This effect is responsible for the optical activity of these nanostructures, resulting in circular dichroism. Relatively simple self-assembly based fabrication of short-range ordered NCR arrays may facilitate the development of new tunable, highly active amorphous metamaterials and photonic devices.

Funding

RFBR (15-03-99582); Danish Research Council (4184-00301B).

Acknowledgments

V.E.B. acknowledges the support from Russian Foundation for Basic Research. G.K. and D.S. acknowledge the funding from the Danish Research Council.

Disclosures

The authors declare that there are no conflicts of interest related to this article.